Modeling and virtual decomposition control with stability analysis for multi-arm-multi-joint space robot

*Xueqian Wang[1,2,3,4,5], Bo Xia[2,4,5], Gang Li[1,2,3], Bin Liang[1,2,3]

[1]*Tsinghua University, National Laboratory for Information Science and Technology, Beijing, China, E-mail: wang.xq@sz.tsinghua.edu.cn*

[2]*Tsinghua University, Graduate School at Shenzhen, Shenzhen, China, E-mail: xb15@mails.tsinghua.edu.cn*

[3]*Tsinghua University, Department of Automation, Beijing, China, E-mail: li.gang@sz.tsinghua.edu.cn*

[4]*Shenzhen Key Lab of Space Robotic Technology and Telescience, Shenzhen, China, E-mail: wang.xq@sz.tsinghua.edu.cn*

[5]*Shenzhen Engineering Lab of Precision Geometry Measurement Technology, Shenzhen, China, E-mail: wang.xq@sz.tsinghua.edu.cn*

ABSTRACT

The research in the paper is to deal with the virtual decomposition control issue with stability analysis for multi-arm-multi-joint space robots. The mathematical model of a multi-arm-multi-joint space robot is firstly built. On the basis of the virtual decomposition control principle, the multi-arm-multi-joint space robot model is virtually decomposed into multiple sub-models from the arm and joint level, and kinematics and dynamics of each sub-model are analyzed. The virtual decomposition controller of each sub-model is designed. The combination of each sub-model and its virtual decomposition controller is a control subsystem of this multi-arm-multi-joint space robot. All control subsystems construct the virtual decomposition control system of the multi-arm-multi-joint space robot. The virtual stability of each control subsystem is analyzed adopting the virtual power flow related to the products of velocity errors and force errors. Based on stability analysis of each control subsystem, the stability for the virtual decomposition control system of the multi-arm-multi-joint space robot is analyzed. Finally, the virtual decomposition control system of the multi-arm-multi-joint space robot is simulated. Simulations and calculations show that this virtual decomposition control system is effective and stable.

1 INTRODUCTION

With development of astronautic technologies, space robots play an increasingly important role in accomplishing on-orbit tasks. However, the system complexity for space robots can cause the difficulty of building entire and precise mathematical models and large calculation workloads of making solutions and control of space robots difficult [1]. Hence, researches on precise modeling and control for space robots are always popular.

Dynamics of space robots is usually modeled using the Lagrange function and Newton-Euler method. Though robot models are improved on the basis of the two approaches, there still exist large solving workloads[2]. Besides, several control methods of space robots have been developed, such as the PID control, the solved force torque control, the robust adaptive control and the adaptive neural network control[3]-[4]. Obviously, these control methods have their advantages and application backgrounds. When multiple degrees of freedom are considered such as a humanoid robot with more than 30 degrees of freedom, it is very difficult to apply these control methods to control robots.

However, the virtual decomposition control (VDC) can be used to control robots with multiple degrees of freedom. According to VDC[5-10], a complex robot system is virtually decomposed into several robot subsystems; dynamics modeling, control and virtual stability analysis of each subsystem are respectively achieved; eventually, control and stability analysis of this entire robot system are completed.

In this paper, the VDC method is adopted to model a dual-arm three-link space robot and control this robot, and simulations show that the VDC method is effective for this robot.

2 MODELING OF SPACE ROBOT

2.1 Model Description under VDC

The planar schematic of a dual-arm robot with three degrees of each arm is shown in Figure 1.

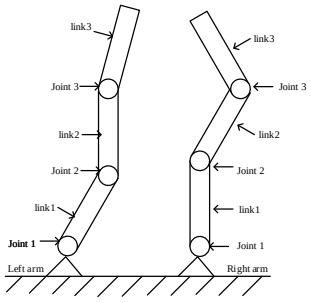

Figure 1: Planar schematic of a dual-arm robot

Without loss of generality, one of two arms is considered. In the paper, the right arm is considered and its schematic is shown in Figure 2. The mass of its ith link is m_i kg, the length of its ith link is l_i m, the distance from the mass center of ith link to ith joint is d_i m and the rotational inertia around the mass center is I_{oi} kg m^2. And for ith joint, the rotational inertia is

I_{mi} kg·m^2 and the ith joint angle is q_i rad. The coordinate system {o} is connected to the end effector of the robot and the x-axis direction is the same as the last link direction.

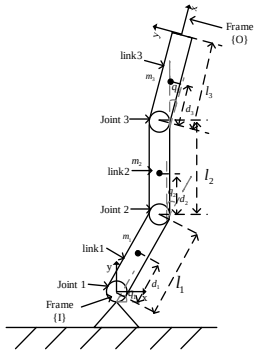

Figure 2: Schematic of the right arm

The description of the system model is divided into five parts as follows[5]-[10]: 1) the system is decomposed virtually into several subsystem; 2) generalized velocities are computed at every subsystem after decomposition; 3) the net force of all links from the base to the end of the arm is computed; 4) the force on the joint is computed from the end of the arm to the base using the net force obtained from 3); 5) based on the previous step, the control torque on the joints can be calculated.

Similarly, the right arm is considered. This arm system is decomposed virtually introducing five cut points. One of subsystems in the right arm with virtual decomposition is shown in Figure 3.

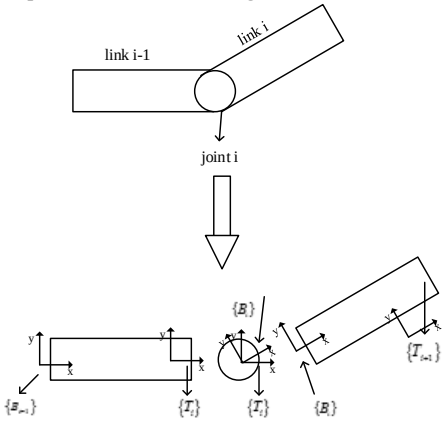

Figure 3 : Virtual decomposition in a subsystem of the right arm

After decomposition of the right arm system, five coordinate systems respectively correspond to the five cutting points. Difference coordinate systems indicate that there is difference for force/torque transfer direction. For example, in {B$_i$} (i=1,2,3), the force/torque transfer direction is from joint i to link i; in {T$_i$} (i=1,2,3), the force/torque transfer direction is from link i-1 to joint i. It can be seen that forced parts in {B$_i$} and {T$_{i+1}$} are link i. Hence, the x-axis direction in {B$_i$} and {T$_{i+1}$} is set to be the direction of link i. Besides, there exists a driving-driven relation between a cutting point and its adjacent subsystem. For {B$_i$}, it is a driven cutting point of link i, and also is a driving cutting point of joint i; For {T$_i$}, it is a driven cutting point of joint i, and also is a driving cutting point of link i+1.

2.2 Generalized Velocities

In a planar, information of linear velocities and angular velocities is necessary to display motion states of a plant. With this consideration, the generalized velocity is defined to be the vector consisting of linear velocities and angular velocities. So the generalized velocity in {B$_i$} is expressed by

$$ {}^{B_1}V = \begin{bmatrix} {}^{B_1}R_I \begin{bmatrix} \dot{x}_{B_1}, \dot{y}_{B_1} \end{bmatrix}^T & \omega_{B_1} \end{bmatrix}^T , $$

where ${}^{B_1}R_I$ is a rotation matrix that transforms a physical vector expressed in frame {I} to the same physical vector expressed in frame {B$_1$}, $\begin{bmatrix} \dot{x}_{B_1}, \dot{y}_{B_1} \end{bmatrix}^T \in R^2$ is linear velocities of the origin in the inertial system, $\omega_{B_1} \in R$ is the angular velocity of link 1.

And velocities in all coordinate systems are as follows.

$$ {}^{B_1}V = z\dot{q}_1 \tag{1} $$

$$ {}^{T_i}V = {}^{B_{i-1}}_{T_i}U^T \, {}^{B_{i-1}}V \tag{2} $$

$$ {}^{B_i}V = z\dot{q}_i + {}^{T_i}_{B_i}U^T \, {}^{T_2}V \tag{3} $$

where $i = 2,3$, $z = \begin{bmatrix} 0,0,1 \end{bmatrix}^T \in R^3$.

2.3 Calculation Net Forces of All Links

2.3.1 Generalized Force

As the definition of generalized velocity, the combination of force and torque is defined as the generalized force vector. For example, the generalized force in {B$_1$} is expressed by

$$ {}^{B_1}F = \begin{bmatrix} {}^{B_1}R_I \begin{bmatrix} f_{B_{1x}} & f_{B_{1y}} \end{bmatrix}^T & m_{B_1} \end{bmatrix}^T , $$

where $\begin{bmatrix} f_{B_{1x}}, f_{B_{1y}} \end{bmatrix}^T \in R^2$ denotes the force vector of link 1 exerted by joint 1 in the inertial system, $m_{B_1} \in R$ represents the torque of link 1 exerted by joint 1 in {B$_1$}.

2.3.2 Dynamic Equations of Links

The link dynamics is denoted by

$$ {}^{B_i}F^* = M_{B_i} \frac{d}{dt}({}^{B_i}V) + C_{B_i}\left({}^{B_i}\omega\right){}^{B_i}V, \tag{4} $$

where i = 1,2,3.

2.4 Force Transmission

From the end of the system to the base, the net force of each link is denoted as follows (i=1,2).

$$ {}^{B_3}F^* = {}^{B_3}F \tag{5} $$

$$ {}^{B_i}F^{*} = {}^{B_i}F - {}^{B_i}U_{T_{i+1}}\,{}^{T_{i+1}}F \tag{6} $$

$$ {}^{T_{i+1}}F = {}^{T_{i+1}}U_{B_{i+1}}\,{}^{B_{i+1}}F \tag{7} $$

Then the force exerted to each joint is

$$ {}^{B_3}F = {}^{B_3}F^{*} \tag{8} $$

$$ {}^{B_i}F = {}^{B_i}F^{*} + {}^{B_i}U_{T_{i+1}}\,{}^{T_{i+1}}F \tag{9} $$

2.5 Calculation of Joint Torque

Ignoring factors such as flexibility, the joint model is built by

$$ I_{mi}\ddot{q}_i + k_{ci}sign(\dot{q}_i) = \tau_i - \tau_{ai} = \tau_i^{*} \tag{10} $$

And the torque exerted by the joint is expressed by

$$ \tau_{ai} = z^{T\,B_i}F \tag{11} $$

So the control torque can be expressed by

$$ \tau_i = \tau_i^{*} + \tau_{ai} \tag{12} $$

where i=1,2,3, $I_{mi} \in R$ denotes the rotational inertia of *i*th joint, $k_{ci} \in R$ is the friction coefficient of *i*th joint, $\tau_i^{*} \in R$ is the static torque of *i*th joint, $\tau_i \in R$ is the control torque of *i*th joint, τ_{ai} is the torque of link exerted by *i*th joint.

3 VIRTUAL DECOMPOSITION CONTROL

There exist errors among practical operations and desired operations, which are caused by external conditions such as environment situations, component quality and internal factors such as precision of model descriptions and human operations during practical operations. To reduce the produced errors, the desired velocity and control error item are added to design a novel velocity such that practical operations can approximate desired operations. Similarly, control laws are devised in the light of the aforementioned five-step method in Session 2.

Considering the motion of arm in the joint space, joint angle velocities are designed by

$$ \dot{q}_{ir} = \dot{q}_{id} + \lambda\left(q_{id} - q_i\right), i = 1,2,3 \tag{13} $$

where q_{id} denote desired joint angles; λ is a control parameter, $\lambda > 0$.

3.1 Virtual Decomposition

According to the virtual decomposition principle in Section 2.1, decomposed frameworks are reserved as the basis in further calculations

3.2 Required Generalized Velocity

From (13), the joint angle required velocities is obtained. Also, from (1)(2)(3), required generalized velocities are as follows based on the three coordinate systems.

$$ {}^{B_1}V_r = z\dot{q}_{1r} \tag{14} $$

$$ {}^{T_i}V_r = {}^{B_{i-1}}U_{T_i}^{T\,B_{i-1}}V_r \tag{15} $$

$$ {}^{B_i}V_r = z\dot{q}_{ir} + {}^{T_i}U_{B_i}^{T\,T_2}V_r \tag{16} $$

where *i*=2,3.

3.3 Required Generalized Force

Net torques of links are contrived by

$$ {}^{B_i}F_r^{*} = Y_i\hat{\theta}_i + K_{Bi}\left({}^{B_i}V_r - {}^{B_i}V\right), \tag{17} $$

where i = 1,2,3,

$$ Y_i\theta_i = M_{B_i}\frac{d}{dt}\left({}^{B_i}V_r\right) + C_{B_i}\left({}^{B_i}\omega\right)^{B_i}V_r\ , $$

$$ \theta_i = \left[m_i, m_i d_i, I_{oi} + m_i d_i^{\,2}\right]^T $$

And, $\hat{\theta}_i \in R^3$ are estimations of θ_i, $K_{Bi} \in R^{3*3}$ are positive definite matrix.

The P-function is adopted to update $\hat{\theta}_i$ as follows.

$$ \hat{\theta}_{i\gamma} = P\left(s_{i\gamma}, \rho_{i\gamma}, \underline{\theta}_{i\gamma}, \overline{\theta}_{i\gamma}, t\right) \tag{18} $$

$$ s_i = Y_i^T\left({}^{B_i}V_r - {}^{B_i}V\right) \tag{19} $$

where $i = 1,2,3$, $\gamma = 1,2,3$, γ is γth element in a corresponding vector, $\rho_{i\gamma} > 0$ represents updated gains, $\underline{\theta}_{i\gamma}$ and $\overline{\theta}_{i\gamma}$ are respectively the low bound and the upper bound of $\theta_{i\gamma}$.

3.4 Force transmission

Compared to (7)(8)(9), the required generalized forces are designed as follows (*i*=1,2).

$$ {}^{B_3}F_r = {}^{B_3}F_r^{*} \tag{20} $$

$$ {}^{B_i}F_r = {}^{B_i}F_r^{*} + {}^{B_i}U_{T_{i+1}}\,{}^{T_{i+1}}F_r \tag{21} $$

$$ {}^{T_{i+1}}F_r = {}^{T_{i+1}}U_{B_{i+1}}\,{}^{B_{i+1}}F_r \tag{22} $$

3.5 Required joint torques

Net torques of joints are solved by (*i*=1,2,3)

$$ \tau_{ir}^{*} = Y_{ai}\left(t\right)\hat{\theta}_{ai} + k_{ai}\left(\dot{q}_{ir} - \dot{q}_i\right) \tag{23} $$

where,

$$ \tau_i^{*} = Y_{ai}\theta_{ai} = I_{mi}\ddot{q}_i + k_{ci}sign(\dot{q}_i), $$

$$ \theta_{ai} = \left[\theta_{ai1} \quad \theta_{ai2}\right]^T = \left[I_{mi} \quad k_{ci}\right]^T. $$

Also, $\hat{\theta}_{ai}$ in (23) is a estimation of θ_{ai}, k_{ai} denotes a feedback gain $\left(k_{ai} > 0\right)$.

Then, link torques from solved outputs are

$$ \tau_{air} = z^{T\,B_i}F_r \tag{24} $$

And control torques are expressed by

$$ \tau_i = \tau_{ir}^{*} + \tau_{air} \tag{25} $$

$\hat{\theta}_{ai}$ is updated using P-function as follows $\left(i = 1,2,3, \gamma = 1,2\right)$.

$$\hat{\theta}_{ai\gamma} = P\left(s_{ai\gamma}, \rho_{ai\gamma}, \underline{\theta}_{ai\gamma}, \overline{\theta}_{ai\gamma}, t\right) \quad (26)$$

$$s_{ai} = Y_{ai}^T \left(\dot{q}_{ir} - \dot{q}_i\right) \quad (27)$$

where $\rho_{ai\gamma} > 0$ represents updated gains, $\underline{\theta}_{ai\gamma}$ and $\overline{\theta}_{ai\gamma}$ are respectively the low bound and the upper bound of $\theta_{ai\gamma}$.

4 STABILITY ANALYSIS

Stability analysis for the control system is accomplished verifying the virtual stability of each subsystem and then analyzing stability of the entire control system based on the stability analysis of each subsystem.

1) Virtual stability analysis of links and joints

For the descriptions about the system (1)-(12) with control laws (14)-(16), (17), (20)-(25) and adjustment equations of adaptive parameters (8), (9), (26), (27), ${}^{B_i}V_r - {}^{B_i}V$ and $\dot{q}_{ir} - \dot{q}_i$ are proved to be virtual functions of L_2 and L_∞ (i=1,2,3) based on relative theories in [5], and these subsystems are virtually stable.

Proof:

The non-negative function of the ith link is represented by v_{li}, and that of the ith joint is represented by v_{ji} (i=1,2,3) such that

$$v_{li} = \frac{1}{2}\left({}^{B_i}V_r - {}^{B_i}V\right)^T M_{B_i}\left({}^{B_i}V_r - {}^{B_i}V\right) + \frac{1}{2\rho_{i\gamma}}\sum_{\gamma=1}^{3}\left(\theta_{i\gamma} - \hat{\theta}_{i\gamma}\right)^2 \quad (28)$$

$$v_{ji} = \frac{I_{mi}}{2}\left(\dot{q}_{ir} - \dot{q}_i\right)^2 + \frac{1}{2\rho_{ai\gamma}}\sum_{\gamma=1}^{2}\left(\theta_{ai\gamma} - \hat{\theta}_{ai\gamma}\right)^2 \quad (29)$$

In view of lemma 1, and the time derivate of (28) become

$$\dot{v}_{li} \le -\left({}^{B_i}V_r - {}^{B_i}V\right)^T K_{Bi}\left({}^{B_i}V_r - {}^{B_i}V\right) + \left({}^{B_i}V_r - {}^{B_i}V\right)^T \left({}^{B_i}F_r^* - {}^{B_i}F^*\right) \quad (30)$$

For the term in (30),

$$\left({}^{B_i}V_r - {}^{B_i}V\right)^T \left({}^{B_i}F_r^* - {}^{B_i}F^*\right),$$

for i = 1,2,

$$\left({}^{B_i}V_r - {}^{B_i}V\right)^T \left({}^{B_i}F_r^* - {}^{B_i}F^*\right) = p_{B_i} - p_{T_{i+1}} \quad (31)$$

and for i=3,

$$\left({}^{B_3}V_r - {}^{B_3}V\right)^T \left({}^{B_3}F_r^* - {}^{B_3}F^*\right) = p_{B_3} \quad (32)$$

where

$$p_{B_i} = \left({}^{B_i}V_r - {}^{B_i}V\right)^T \left({}^{B_i}F_r - {}^{B_i}F\right)$$

$$p_{T_i} = \left({}^{T_i}V_r - {}^{T_i}V\right)^T \left({}^{T_i}F_r - {}^{T_i}F\right)$$

that denotes the virtual power flow at different cutting points.

(33)(34) are obtained in terms of (27-29).

For i =1 , 2

$$\dot{v}_{li} \le -\left({}^{B_i}V_r - {}^{B_i}V\right)^T K_{Bi}\left({}^{B_i}V_r - {}^{B_i}V\right) + p_{B_i} - p_{T_{i+1}} \quad (33)$$

and for i = 3

$$\dot{v}_{l3} \le -\left({}^{B_3}V_r - {}^{B_3}V\right)^T K_{B_3}\left({}^{B_3}V_r - {}^{B_3}V\right) + p_{B_3} \quad (34)$$

According to (33)(34), virtual stability of links can be defined.

Also, for (29),

$$\dot{v}_{ji} \le -k_{ai}\left(\dot{q}_{ir} - \dot{q}_i\right)^2 + \left(\dot{q}_{ir} - \dot{q}_i\right)\left(\tau_{ir}^* - \tau_i^*\right) \quad (35)$$

where

$$\left(\dot{q}_{ir} - \dot{q}_i\right)\left(\tau_{ir}^* - \tau_i^*\right) = -\left(\dot{q}_{ir} - \dot{q}_i\right)\left(\tau_{air} - \tau_{ai}\right).$$

For i = 1,

$$-\left(\dot{q}_{1r} - \dot{q}_1\right)\left(\tau_{a1r} - \tau_{a1}\right) = -p_{B_1} \quad (36)$$

And for i = 2, 3

$$-\left(\dot{q}_{ir} - \dot{q}_i\right)\left(\tau_{air} - \tau_{ai}\right) = -p_{B_i} + p_{T_i} \quad (37)$$

(38)(39) are achieved according to (35)-(37).

For i = 1,

$$\dot{v}_{j1} \le -k_{a1}\left(\dot{q}_{1r} - \dot{q}_1\right)^2 - p_{B_1} \quad (38)$$

And for i= 2, 3

$$\dot{v}_{ji} \le -k_{ai}\left(\dot{q}_{ir} - \dot{q}_i\right)^2 - p_{B_i} + p_{T_i} \quad (39)$$

According to (38)(39), virtual stability of links can be defined.

End

2) Stability analysis of the entire control system

Proof:

Construct the non-negative function:

$$v = \sum_{i=1}^{3} v_{li} + \sum_{i=1}^{3} v_{ji} \tag{40}$$

and

$$\dot{v} \le -\sum_{i=1}^{3} \left({}^{B_i}V_r - {}^{B_i}V \right)^T K_{B_i} \left({}^{B_i}V_r - {}^{B_i}V \right) - \sum_{i=1}^{3} k_{ai} \left(\dot{q}_{ir} - \dot{q}_i \right)^2 \tag{41}$$

In the light of Lemma 2.3, (42)(43) hold (i=1,2,3).

$${}^{B_i}V_r - {}^{B_i}V \in L_2 \cap L_\infty \tag{42}$$

$$\dot{q}_{ir} - \dot{q}_i \in L_2 \cap L_\infty \tag{43}$$

In the light of (13) and Lemma 2.4, (44)(45) hold (i=1,2,3).

$$\dot{q}_{id} - \dot{q}_i \in L_2 \cap L_\infty \tag{44}$$

$$q_{id} - q_i \in L_2 \cap L_\infty \tag{45}$$

Hence,

$$q_{id} - q_i \to 0 \tag{46}$$

End

5 SIMULATION

The dual-arm three-link robot system with VDC is simulated. Simulation parameters are shown in Table 1.

In order to carry an on-orbit object from a position to another position, the right arm moves in a large range and the left arm does in a small scale, and the two arms of this robot work coordinately. Desired joint trajectory equations of the left arm are given in Table 2, and desired joint trajectory equations of the right arm are given in Table 3.

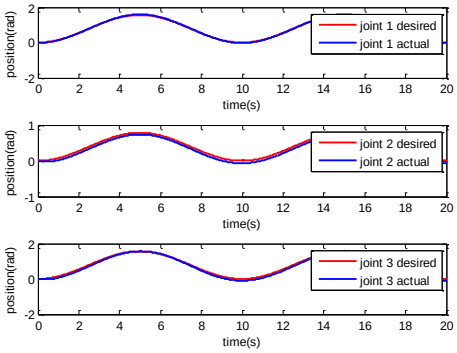

Figure 4 : Joint trajectory tracking curves of the right arm

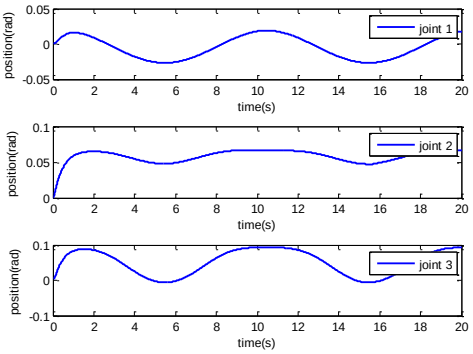

Figure 5 : Joint trajectory tracking errors of the right arm

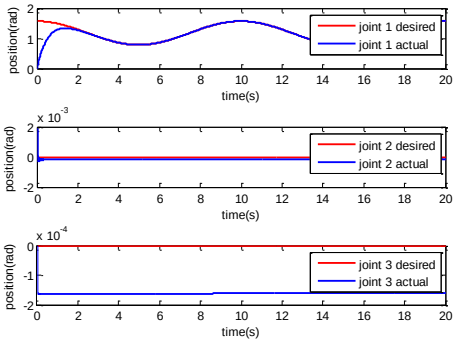

Figure 6: Joint trajectory tracking curves of the left arm

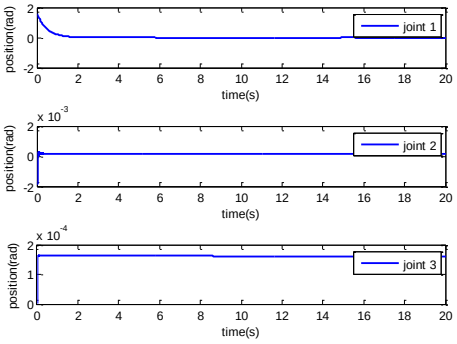

Figure 7: Joint trajectory tracking errors of the left arm

Simulation figures are provided in Figure 4-7. Joint trajectory tracking curves of the right arm are shown in Figure 4 and joint trajectory tracking errors of the right arm are shown in Figure 5; joint trajectory tracking curves of the left arm are shown in Figure 6 and joint trajectory tracking errors of the left arm are shown in Figure 7. From Figures 4-7, it can be observed that the output of each joint for the right or left arm can follow the corresponding desired joint trajectory with small and acceptable tracking errors.

After solving trajectories of all joints of this robot, the output trajectory of the robot end effector is obtained and shown in Figure 8.

Table 1 Simulation parameters (International unit)

	Link 1			Joint 1		Link 2			Joint 2		Link 3			Joint 3	
	m	L	I_o	kc	I_m	m	L	I_o	kc	I_m	m	L	I_o	kc	I_m
Left arm	10	0.5	1	0.4	2	10	0.5	1	0.4	2	10	0.5	1	0.4	2
Right arm	10	0.5	1	0.4	2	10	0.5	1	0.4	2	10	0.5	1	0.4	2

Table 2 Desired joint trajectory equations of the left arm

Joint	Trajectory equations
Joint 1	$3*pi/8-pi/8*\sin(\mathrm{pi}*t/5-\mathrm{pi}/2)$
Joint 2	0
Joint 3	0

Table 3 Desired joint trajectory equations of the right arm

Joint	Trajectory equations
Joint 1	$pi/4-pi/4*\sin(\mathrm{pi}*t/5-\mathrm{pi}/2)$
Joint 2	$pi/8-pi/8*\sin(\mathrm{pi}*t/5-\mathrm{pi}/2)$
Joint 3	$pi/4-pi/4*\sin(\mathrm{pi}*t/5-\mathrm{pi}/2)$

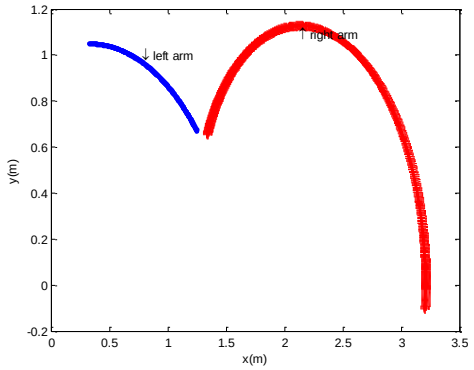

Figure 8: Output trajectory of the robot end effector

6 Conclusion

The research on the multi-arm-multi-joint space robot control is still popular. As far as multi-arm-multi-joint space robots are concerned, the increasing number of the arm and joint can cause cumbersome calculations and complex coupling dynamics which enhance the difficulty of the control design for multi-arm-multi-joint space robots. Generally speaking, it is difficult to adopt traditional control methods to tackle the multi-arm-multi-joint space robot control issue. However, the virtual decomposition control theory is suitable for the high-precision control of multi-arm-multi-joint space robots with variable dynamics parameters.

In the paper, the satisfied control issue for dual-arm three-link space robots is dealt with adopting VDC approach from the theory and simulation level. On the basis of know robot dynamics and subsystem dynamics, the VDC approach is applied as 1) an original robot system is decomposed virtually into several subsystems, and dynamics and kinetics of this robot system are deduced and analyzed; 2) according to the aforementioned virtual decompositions, generalized velocities and generalized forces are subsequently devised so that the output velocities approximate practical velocities; 3) the stability of the designed robot control system is guaranteed introducing the virtual power flow for which velocity errors multiply force errors. Simulations show that practical positions of each joint adequately approach desired positions of each joint with small tracking errors.

Consequently, this investigation verifies that the virtual decomposition control is a feasible approach of handling the multi-arm-multi-joint space robot control problem.

Acknowledgement

The authors would like to thank anonymous reviewers for their valuable comments. The work is funded by National High Technology Research and Development Program of China (863 Program)

(No.2015AAXX46611) and China Postdoctoral Science Foundation (No.20159200078).

References

[1] Liu Chang'an and Li Guodong (2002) Research summarizing of free flying space robot. *Robot* 24(4):380-383.

[2] Liu Bo-xun (1989) Research summarizing of robot dynamics. *Mechanics and Engineering*, (03): 11-20.

[3] Zhang Wenhui and Zhu Yinfa (2013) Overview of the research on control methods of the space robots. *Journal of Shandong University of Science and Technology*, 32(3):12-21.

[4] Ding Xuegong (2007) *Research on the control method of the robot*. Hang zhou, IL: University of Zhejiang Press.

[5]Zhu Wenhong (2010)*Virtual Decomposition Control (STAR Series, no. 60).*New York, NY, USA: Springer-Verlag.

[6]Zhu Wenhong and T. Lamarche (2007) Modular robot manipulators based on virtualdecomposition control.In: proceedings of 2007 IEEE international conference on robots and automation, Rome, Italy, pp.2235–2240.

[7] Zhu Wenhong and XiYugeng (1997) Virtual decomposition based control for generalized high dimensional roboticsystems with complicated structure.In: proceedings of 1997 IEEE Transactions on robots and automation, pp.411–436.

[8]Zhu Wenhong and J.De Schutter (1999) Adaptive control of mixed rigid/flexiblejoint robot manipulators based on virtual decomposition.In: proceedings of 1999 IEEE Transactions on robots and automation, pp.310–317.

[9]Zhu Wenhong (2010) FPGA-based adaptive friction compensation for precisioncontrol of harmonic drivers.In: proceedings of 2010 IEEE Transactions on robots and automation,Anchorage, AK, USA, pp.4657–4662.

[10]Zhu Wenhongand J.De Schutter (1999)Control of two industrial manipulatorsrigidly holding an egg. In: proceedings of 1999 IEEE conference on control system, pp.24–30.